Kaolinite/Polypropylene Nanocomposites. Part 3: 3D Printing

Kilole Tesfaye Chaka[1], Luca Fambri[2], Nalankilli Govindan[3]

[1]Lecturer, Basic science and Engineering Research and Innovation Centre
[3]Professor, Textile Chemistry Research and Innovation Centre
[1,3]Ethiopian Institute of Textile and Fashion Technology (EiTEX), Bahir Dar University, Bahir Dar, Ethiopia
[2]Professor, Department of Industrial Engineering, Trento University, Italy

---

Abstract - *Polypropylene (PP) is the most widely used semi-crystalline thermoplastic polymers due to its good thermal and mechanical properties, high dimensional stability and excellent processability. In this research three types of different molecular weight PP named HP500 (HP), Atofina HG265FB (ATO) and Borealis PPH7089 (B) were used for production of nanocomposites at different kaolinite contents. HP and its nanocomposites were extruded filaments for 3D printing and measured density of filaments show lower theoretical density due to cavity and other defects as observed in FESEM micrographs. TGA analysis shows thermal decomposition temperature increases with increasing kaolinite content. HP and its composite were able to be 3D printed by coating of 3D printer bed with PP which improves poor adhesion behaviour of PP and it's composite on heated bed. Mechanical properties of 3D printed sample shows lower value due to large cavity formation between layers in the structure. DSC of 3D printed sample reveals crystallization temperature increase with kaolinite content and crystallinity content doesn't change after filaments productions.*

Key words: Polypropylene, Nanocomposites, kaolinte, 3D Printing, Mechanical properties, DSC, TGA

1. INTRODUCTION

3D Printing, also known as additive manufacturing or desktop fabrication, is a process where in a solid three-dimensional object is printed layer by layer from raw material, which could potentially lead to a whole new era in manufacturing. Plastics are the most widely used materials in additive manufacturing, and the important ones are acrylonitile butadiene styrene (ABS), polylactic acid (PLA), polyvinyl alcohol (PVA) and polycarbonate (PC) which requires high-temperature nozzle design.

The manufacturing process begins with a 3D model of the object, usually created by computer-aided design (CAD) software or a scan of an existing artifact and building objects layer-by-layer [1]. Specialized software slices this model into cross-sectional layers, creating a computer file that is sent to the 3D printing machine. This machine then creates the object by forming each layer via the selective placement (or forming) of material. This technology attracts strong interest from both industry and academic for the challenging possibility to build objects with complex shapes and minimal use of harmful chemicals at a reasonable speed [2,3]. There are several 3D printing processes that are differentiated by the manner in which they create each layer. One technique known as Fused Filament Fabrication is shown in fig.1.

The distinct advantages of 3D printing processes are its capability to build complex geometries that cannot be fabricated by any other means i.e. it offers the most geometrical freedom in engineering design. Consequently, new opportunities exist for design in industries as diverse as automotive, aerospace, and bio-engineering. It is possible to create functional parts without the need for assembly, saving both production time and cost.

Fused Filament Fabrication, Fig.1 involves extruding thermoplastic material through heated nozzles to create a part's cross sections. Filament feedstock is guided by a roller into a liquefier that is heated to a temperature above the filament's melting point. The material is then able to flow freely through the nozzle. When the material reaches the substrate, it cools and hardens. Once the layer is complete, the build platform is lowered one layer-thickness by the Z-stage and deposition of the next layer begins. A secondary sacrificial material may also be deposited (and later removed) in order to support the construction of overhanging geometries.

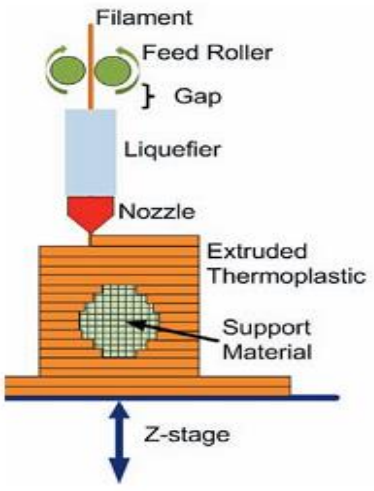

Fig.1 Fused filament fabrication [4].

Currently, FDM is the technique showing the higher potential for product manufacturing, with the capability to compete with conventional polymer processing techniques [5,6]. Most of the published studies up to now focused little on the extrusion processing window used in the production of filaments with suitable diameter and homogeneity for FDM. The use of commercially available filaments, used in the majority of the published studies, limits them to the inherent characteristics of the FDM process [7]. Moreover, the comparison either at the morphological and mechanical level of the parts produced by FDM and by conventional techniques would be more authentic if the material used to produce the parts were to be the same in both processes. Literature lacks studies that follow the FDM process from the start, i.e., from the filament production, allowing an absolute control of the processes and a true comparison between competing techniques [8].

Carneiro et al [9] addresses the potential of polypropylene (PP) as a candidate for fused deposition modelling (FDM), starting with the PP pellets, filament extrusion and test samples printing. Adding nanomaterials such as carbon nanotubes, nanowires, and nanoparticles to matrices such as polymers, metals, and ceramics via AM has the potential to improve the performances of the resulting components [5,10].

2. MATERIALS AND METHODS

2.1 Fused deposition modelling (FDM)

3D printed specimens were manufactured by a Sharebot Next Generation Desktop 3D printer (Sharebot NG, Italy) feed with the extruded filaments of about 1.7mm diameter. Here sample of HP, K10-HP and K20-HP filaments are used to feed a 3D printer. As-spun filament of 1.7 mm is fed to the 3D printer to re-melt and extrudes through the heated nozzle which has size of about 0.35mm. Fig.2 shows the top view of desktop 3D printer during printing process in progress.

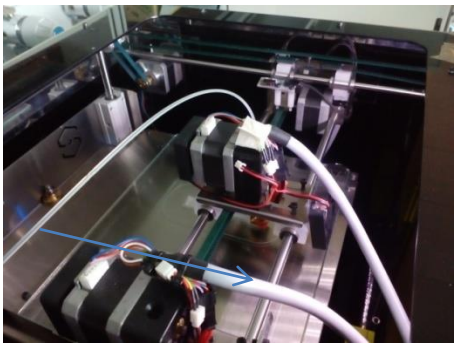

Fig. 2 Top view of Sharebot Next Generation Desktop 3D Printer [11].

Schematically representation in Fig.3 shows dumbbell and single filament specimens built-up along horizontal orientations. In this figure X is the direction of filament deposition and Z is the direction of the overlapping layers.

Infill types of concentric and maximum fill percentage were used in Slic3r software along with the following printing parameters: concentric type of infill, object infill 100%, nozzle diameter 0.35 mm, layer height 0.20 mm. All other processing parameters and size of FDM specimens are summarized in Table 1.

Sample Type		Neat HP500	HP500/10 K	HP500/20 K
Diameter (mm)		1.70	1.70	1.70
Temp. (^{0}C)	Extruder	240	230	225
	Bed	90	80	75

As the content of kaolinite increases in PP-K nanocomposites the working temperature is decreasing (Table 1b) because melt flow was increasing with kaolinite content as observed from MFI results.

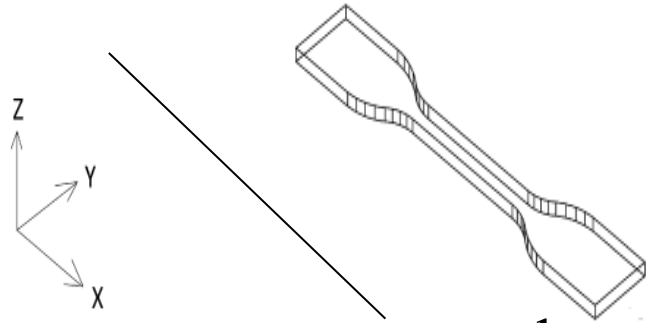

Fig. 2.1. Schematic of (a) single filaments from 3D-printer (b) 3D printed dumbbell specimens at horizontal orientations.

Table 1 Parameters for 3D printing of neat PP and PP-K nanocomposites (a) Printing setting (Layers and perimeters, Infill, Speed) (b) filament setting

Layer height	0.2 mm
First layer height	0.2 mm or %
Perimeter (minimum)	2
Fill density	1
Fill pattern	concentric
Infill every	1
Fill angle	45^0
Solid infill threshold area	100 mm^2

Perimeters	20mm/s
Small perimeters	10 mm/s or %
External perimeters	15 mm/s or %
Infill	20 mm/s
Support material	25 mm/s
Gap fill	20 mm/s
Speed for non-print moves (Travel)	25 mm/s
First layer speed	50% mm/s or %
Cooling Fan speed	100

(a)
(b)

2.2 Testing and Charecterisation

Melt Flow Index measurements were performed by a Dynisco LMI 400 plastometer according to ASTM D1238-10. Scanning electron micrographs (SEM) were observed on a fractured surfaces of specimens immersed in liquid nitrogen through a Carl Zeiss AG Supra 40 field emission scanning electron microscope (FESEM), operating at an acceleration voltage of 3 kV. XRD analysis was performed by using Laue camera for transmission diffraction and over 2θ = 3–50° in the Bragg-Brentano configuration. Dynamic mechanical thermal analysis (DMTA) was performed on as-spun and drawn fibers with a DMA Q800 testing unit (TA Instruments) under tensile mode testing. The FTIR spectra were recorded by Spectrum-One equipped with an UATR (Universal Attenuated Total Reflectance) accessory for PP, kaolinite and its composite samples in a laboratory maintained at relative humidity of 48±2% and 23±1^{0}C.

Thermal Analysis was performed in a temperature range of 30 °C to 700 °C by a TGA Q5000-IR from TA Instruments on sample of about 14 mg at heating rate of 10°C/min tested in both air and nitrogen atmosphere at a flow rate of 100 ml/min. Density measurements were performed by using a Micrometrics Accupyc 1330 helium pycnometer at 23.0°C in a testing chamber of 1 cm^3 and 100 measurements for each specimen. Differential scanning calorimetry (DSC) analysis was performed on samples of about 14 mg in 160 μL aluminium crucible by using a Mettler DSC30 calorimeter in the range of 0–220°C with a heating – cooling – heating cycle at ±10°C/min flushing nitrogen at 100 mL/min. Mechanical properties of fibers and 3D printed dumbbell were performed at room temperature by using an Instron 4502 dynamometer, equipped with load cells of 100 N and 1kN, respectively. Elastic modulus was determined as a secant value between deformation levels of 0.05 and 0.25% according to ISO 527 standard.

3. RESULTS AND DISCUSSIONS

3.1 Additive Manufacturing (3D Printing)

Selected compositions for 3D printing were considering compounded formulations of $F_{20\text{-}21}$ for neat HP, $F_{22\text{–}23}$ for K10-HP and $F_{24\text{–}25}$ for K20-HP (Part 1 of our paper) after understanding the working capability of those compositions in fibers processing. Compounded samples of neat HP and K-HP nanocomposites are used for extrusion of filaments for 3D printing after grinding in to small sizes of about 2mm.Filaments with a diameter of about 1.7 mm are extruded for neat HP and HP-kaolinite nanocomposites. Extruded filaments MFI are tested to see the influence of kaolinite content and extrusion process on the flowability. Then it was analysed by TGA in N_2 gas and air atmosphere to analyse the effect of kaolinite on the thermal stability of HP at different content and density measurement to see the effect of kaolinite content on density of HP polypropylene.

Extruded filaments for 3D printing are used to feed 3D printing machine in which there is re-melting and re-orientation was taken place in nozzle and a microfilament of about 0.35 mm were printed. Then the comparison between filaments for 3D printing (diameter about 1.7 mm) and 3D printed micro filament of (diameters about 0.35 mm) were compared. Thus analyzing by DSC was performed to investigate crystallization behaviour and crystallinity content and mechanical properties are analysed by Quasi-static tensile tests. FESEM and TEM were used to evaluate dispersion of kaolinite in polypropylene on the fractured surfaces of the nanocomposites while XRD was used to monitor kaolinite crystal structure in the PP matrix as well as changes in the crystallinity of HP polypropylene in the nanocomposites.

3D printed dumbbell shape samples was also produced according to the parameters set for printing of neat HP and K-HP described in experimental procedure. Investigated techniques to improve the printability of dumbbell shape specimens, mechanical properties and morphology of produced samples will be discussed in this section.

3.2 Filaments Extrusion and Analysis

The scope of this section is to investigate the sample of HP, K10-HP and K20-HPnanocomposites filaments to show the printability of PP nanocomposites. Filaments of neat HP and HP-kaolinite nanocomposites with a diameter of about 1.7 mm were extruded. Filaments for 3D printing were extruded by using a die of 3.00 mm diameters. The rate of extrusion of filaments for 3D printing is described in Table 2.

Table 2. Parameters set for extrusion of filaments for 3D printing.

Type of filaments	Neat HP	K10-HP	K20-HP
Screw speed (rpm)	40	15	15
Residence time (min)	6	7-8	5
Rate of extrusion (cm/sec)	4.29±0.11	3.10 ± 0.05	3.67 ± 0.03
Rate of collection (g/sec)	0.101 ± 0.003	0.07 ± 0.003	0.086 ± 0.003
Collector speed (number)	5, 6	4	4, 5

A measurement of extrusion rate for K20-HP was difficult due to its high flowability. Reducing the speed of screw was tried but decreasing the speed further cannot give an output required to give about 1.7 mm diameters filaments. Extruded filaments are collected manually after passing through a cold water and collector.

Average diameter of extruded filaments for 3D printing were summarised in Table 3. Apparent draw ratio (ADR) can becalculated according to Equation 1 as the ratio between the cross sectional area of the extrusion die (S_D) and the cross sectional area of the filament (S_F), where cross sectional area of the extrusion die (S_D) used is 3.00 mm.

$$ADR = S_D/S_F \text{..... Eq.1}$$

Table 3. Apparent draw ratio of filaments for 3D printing.

Sample type	Filament diameter (mm)	ADR
Neat HP	1.77 ± 0.09	2.87
K10-HP	1.71 ± 0.05	3.08
K20-HP	1.73 ± 0.06	3.01

3.3 Melt Flow Index

Before testing of melt flow extruded filaments of neat HP and HP-kaolinite nanocomposites with a diameter of about 1.7 mm were cut into small pieces manually by cutter with length of about 2-5mm. Then melt flow index of filaments for 3D printing of neat HP and HP-kaolinite nanocomposites at various kaolinite content were tested in melt flow indexer at temperature of 230 ^{0}C and weight of 2.16 Kg with melting time of 5 minutes. MFI results of neat HP, K10-HP and K20-HP filament for 3D printing was summarized and the results obtained were compared with the MFI of compounded sample at the same conditions (Table 4).

Table 4. Comparison of MFI of filaments for 3D printing with compounded sample.

Sample type	*MFI of filament for 3D printing (g/10min)*	*MFI of compounded sample (g/10min)*
Neat HP	1.96 ± 0.07	1.85 ± 0.14
K10-HP	2.39 ± 0.16	2.00± 0.11
K20-HP	2.46 ± 0.34	2.95± 0.23

It should be noted that the MFI values increased with the percentage of kaolinite in the polymer matrix, with an almost linear dependence on the PP-kaolinite composition. Comparing melt flow index obtained results of filaments for 3D printing with compounded sample shows increase for neat HP and K10-HP while it decreases for K20-HP. These results show that neat HP polypropylene has high viscosity than K-HP nanocomposites and it is possible to understand that 3D printing temperature of neat HP should be higher than that of kaolinite filled HP nanocomposites.

3.4 DSC Analysis of filaments for 3D printing

DSC analysis of neat HP, K10-HPand K20-HP was performed on filaments for 3D printing to provide quantitative evaluation of the crystallization behaviour. The crystallization behaviour of all samples wasstudied at 10 ^{0}C/mincooling rates. The DSC thermograms curves of neat HP, K10-HP and K20-HP filaments for 3D printing are shown in Fig.4.

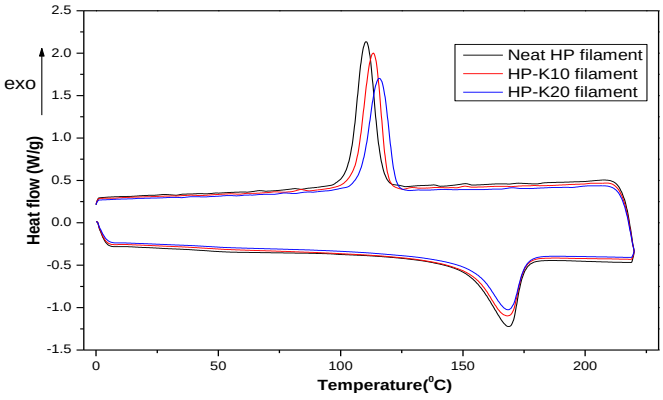

Fig. 4. DSC thermograms of neat HP, K10-HP and K20-HP filaments for 3D printing

From DSC curves some useful parameters for crystallization analysis, such as the melting temperature (Tm), the crystallization temperatures, e.g. the exothermic peak maxima and the end temperature of crystallization can be

obtained. The degree of crystallinity (χ_c) of neat HP and HP-K nanocomposites was calculated.

Considering the results in Table 5, melting temperatures (Tm) have almost the same values for neat HP and K-HP nanocomposites both on first heating and second heating. From the DSC cooling stage, it was noticeable that crystallization temperatures of kaolinite filled filament were higher than for neat PP, i.e. up to 119.1°C for K20-HPversus 113.4^{0}C for neat HP filaments. This clearly implies that the incorporation of kaolinite results in the heterogeneous nucleation to the PP matrix. Also it was observed that crystallinity content of filaments after cooling is higher than the first melting crystallinity displayed. This earlier crystallization phenomenon can be interpreted as the result of an increase in nucleation activities.

Table 5. Results of the DSC analysis: melting temperature (Tm), crystallinity content (Xc) and crystallization temperature (Tc) for neat HP, K10-HP and K20-HP filaments for 3D printing.

Sample Compositions	*1st melting temp.*		*Crystallization temp.*		*2nd melting temp.*		*Crystallinity Content (%)*	
	peak (°C)	*integral (J/g)*	*peak (°C)*	*integral (J/g)*	*peak (°C)*	*integral (J/g)*	*1st Melting*	*After Cooling*
Neat HP	167	83	113	967	165	97	40	47
K10-HP	167	81	116	87	165	87	42	45
K20-HP	166	74	119	78	166	78	43	45

Crystallization temperatures increases with the increase of kaolinite content, and melting temperature and crystallinity content after cooling is almost the same for neat HP and K-HP nanocomposites in both types of filaments. Melting process induces the molecular chains mobility of PP, and reduces the free energy barrier for crystallites formation which is able to accelerate the rate of crystallization. At an early stage of crystallization, the molecular chains of PP might be in contact with the filler surface and limit the movement of polymer chains. The movement of polymer chains which is in a form of distorted network can be quickly relaxed and re-established. This scenario helped to increase the structural stability of polymer matrix giving an increase in the crystallization peak temperature. These findings confirm that kaolinite behaves as a nucleating agent in polypropylene.

3.5 TGA and Density Measurement

Representative TGA analysis ofneat HP, K10-HP and K20-HP of filaments for 3D printing performed in nitrogen gas and in air atmosphere were reported in Fig.5. In these curves it is possible to observe three different zones. The first zone (30°C to 325°C) in N_2gas and (30°C to 250°C) in air atmosphere shows no significant weight loss. In the second zone (325°C to 475°C) in N_2 gas and (250°C up to 430°C) in air atmosphere, a high mass loss is shown due to thermal decomposition of polymer matrix. The last and third zone is between temperature zone of (475°C to 700°C) in N_2gas and (430°C up to 700°C) in air atmosphere. In this temperature zone, since the residuals are not decomposed in both N_2 gas and air atmosphere there is no significant mass loss. The decomposition of the matrix in N_2 gas starts at higher temperature compared to air atmosphere because it is an inert gas that facilitate controlled degradation and prevent undesirable chemical reactions from taking place.

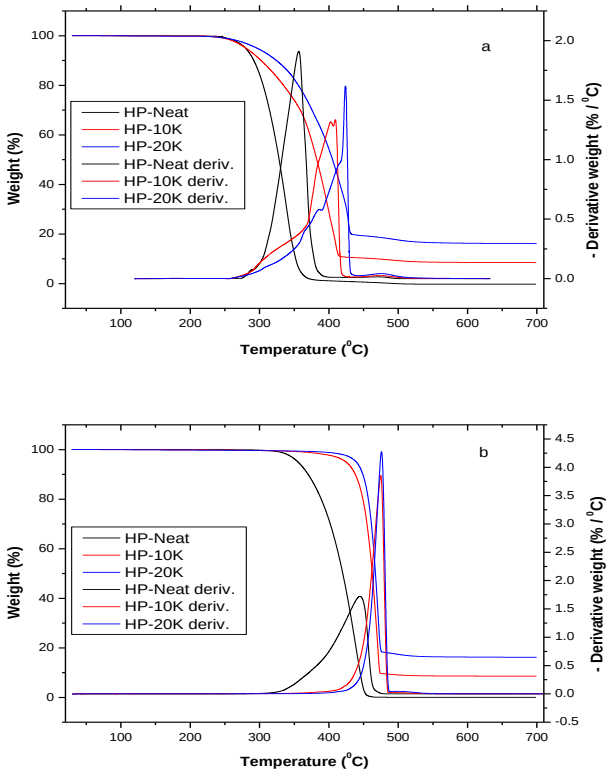

Fig.5 TGA curves and its derivatives of neat HP, K10-HP and K20-HP filaments for 3D printing under (a) Nitrogen gas and (b) air atmosphere.

The main important results in the analysis of TGA for characterization of thermal stability which are thermal decomposition temperatures at 5% and 10% of the weight loss (T_5 and T_{10}), the temperature at maximum rate of the weight loss (T_{dm}, read as the temperature of the corresponding to derivate curves), and the residue (R) at temperature of 700°C are shown in Table 6.

Based on the TGA results, it is possible to conclude that, the thermal decomposition temperature (T_5, T_{10} and T_{dm}) of the PP nanocomposites increases with increasing kaolinite content. This effect results due to kaolinite act as physical barriers to hinder the transport of volatile decomposed products out of the PP nanocomposites during thermal decomposition [12]. The effect is more relevant at the temperature of maximum rate of mass loss, where degradation temperature is about 64 - 88 ^{0}C in air and 27 – 29 ^{0}C in nitrogen higher than that of neat HP, found for compositions at 10 and 20 wt% kaolinite respectively. The residual mass at 700°C was almost equal in both testing medium which is about 8.5% for K10-HP and 16.2% for K20-HP samples. This implies that incorporation of kaolinite into the polymer matrix enhances the thermal stability of polypropylene nanocomposites.

Table 6 TGA results of HP and HP-kaolinite nanocomposites decomposition temperatures at 5%, 10% and maximum rate of the weight loss (T_5, T_{10} and T_{dm}) and residue (R) at temperature of 700°C in air and nitrogen testing medium.

Processing gas	Nitrogen gas				Air atmosphere			
Materials	T_5 [°C]	T_{10} [°C]	T_{dm} [°C]	R [%]	T_5 [°C]	T_{10} [°C]	T_{dm} [°C]	R [%]
Neat PP	353	369	440	0	278	291	339	-0.2
HP-10K	422	437	467	8.5	277	300	403	8.5
HP-20K	438	448	469	16.2	292	323	427	16.2

Density properties of filaments for 3D printing of neat HP and K-HP nanocompositeswere measured by Pycnometer. The results obtained were compared with the theoretical density calculated according to Equation 2 given above;

$$\rho_c = \frac{\rho_f \rho_p}{\rho_p m_f + \rho_f (1 - m_f)} \quad \ldots\ldots\ldots Eq.2$$

Here the theoretical density of K-HP nanocomposites were calculated by taking the density of HP500 polypropylene 0.905 g/cm^3 and density of kaolinite as 2.630 g/cm^3 according the given formula. Measured densities by Pycnometer and calculated were shown in Table 7.

Table 7 Pycnometer measured versus theoretical densities of neat HP, K10-HP and K20-HP nanocomposites filaments for 3D printing.

Sample type	*Density from Pycnometer (g/cm^3)*	*Theoretical density (g/cm^3)*
HP neat	0.8918 ± 0.0004	0.9050
K10-HP	0.9516 ± 0.0017	0.9584
K20-HP	0.9854 ± 0.0022	1.0126

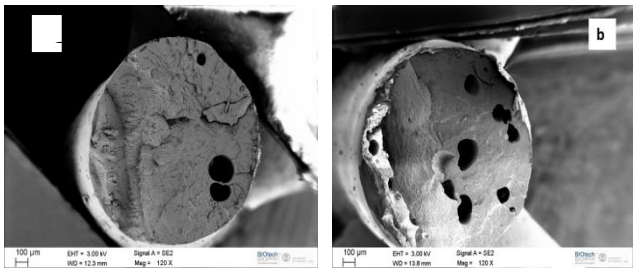

Fig.6 FESEM micrographs of the fractured surface of kaolin-filled HP filaments for 3D printing (X120,000) (a) K10-HP (b) K20-HP.

As it is shown in the table the density of the filaments increases with increase in kaolinite content, in which the results of 0.8918 g/cm^{3}for neat HP polypropylene and the density of 0.9854 g/cm^3 for K20-HP were measured. Also it was observed from the table above pycnometer measured density is lower than expected density (theoretical density) may be due to inclusions of cavity resulting from poor mixing, defects or poor wetting of the filler surface by the polymer. This could be further investigated by FESEM morphologies shown in Fig.6.

Density could be influenced from various factors other than kaolinite content, for instance from the orientation, cavity and from the crystallinity. Fig.6 from FESEM reveals the existence of holes and subsequent plastic deformation in the morphology of kaolin-filled nanocomposites. This is due to weak interfacial adhesion between PP and kaolinite. The amount of holes also implies the content of kaolinite, i.e. the numbers of holes formed in K20-HP is much higher than that of K10-HP. The amount of holes formed directly affects density of filaments; accordingly the difference in density between pycnometer measured and theoretical density is smaller in case of K10-HP (0.0068) than that of K20-HP (0.0272). During the deformation process of particulate-filled polymer composite, the most common failure mechanism is debonding at the filler-matrix interface. From

the micrographs (Fig.6), debonding process of kaolinite aggregates created large holes, which means that kaolinite filler can be pulled out completely from the PP matrix through the interfacial failure as the filler-matrix adhesion is relatively weak. The reason for poor adhesion between kaolinite and PP was probably because of the difference in surface free energy (or polarity).

3.6 Production of 3D Printed Samples (Microfilaments) and Characterization

Polypropylene is a semi-crystalline material, which doesn't follow the normal rules for warping prevention. An amorphous polymer like ABS or PET are able to slowly flow or creep until it cools below the glass transition point, T_g during 3D printing. This means that stresses caused by thermal contraction will shake-out above T_g and only start accumulating when the print cools below T_g and fully solidifies. However, when extruding semi-crystalline polymers like PP in 3D printing, crystallization starts as soon as the temperature drops below the melting point, T_m. PP and its nanocomposites will not flow or creep at a rate that is meaningful over the duration of fused deposition print, and the thermal contraction stresses will simply build up more as it is cooled further below T_m.

Before starting production of 3D printing dumbbell model was built by using CAD and it was sliced into cross-sectional layers by specialized software *slic3r*, creating a computer file that was sent to the 3D printing machine. The 3D printing machine then creates the object by forming each layer via the selective placement of material. Filaments from 3D printer (microfilaments) of 0.35 mm and dumbbell shape sample were shown in Fig.7. From this figure it is possible to see the edge layers and fillings at an angle of 45^0 perpendiculars to each other.

Fig.7 3D printed sample of K10-HP dumbbell and microfilaments.

3.7 Production of Microfilaments

To distinguish from filaments for 3D printing of about 1.7 mm diameter (code F), filaments from 3D printer of 0.35 mm diameter nozzle were given code microfilaments (code μF). Microfilaments extruded through 3D printer are not circular due to flattening of filaments during extrusion through narrow space between nozzle and printer bed. The filament forms like a trapezoid structure and its equivalent diameter are observed by microscope at different direction and measured by using imageJ software. An image of microfilaments observed by rotating in different directions under microscope and measured by ImageJ was shown in Fig.8 for K10-HP microfilament.

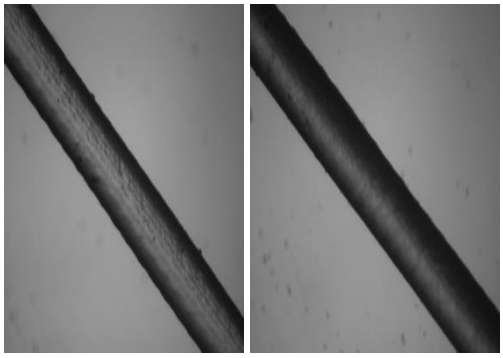

Fig.8 Optical microscope images of 3D printed filament of K10-HP.

Filament diameters were measured at least on three places in each direction and final equivalent diameter was calculated as average of measured value in each direction. Table 8 summarizes equivalent diameters of filaments measured in several directions.

Table 8 Representative equivalent diameters of microfilaments measured by imageJ integrated optical microscope.

Sample type	*Filaments numbers*	*Equivalent diameter*
Neat HP	1	0.441 ± 0.013
	2	0.472 ± 0.014
	3	0.486 ± 0.038
K10-HP	1	0.382 ± 0.015
	2	0.393 ± 0.006
	3	0.354 ± 0.033
K20-HP	1	0.410 ± 0.097
	2	0.400 ± 0.035
	3	0.464 ± 0.028

3.7 Microfilament Characterization

In the following section characterization of microfilaments by different techniques was discussed and its results were compared with the results of filaments for 3D printing. Accordingly the comparison by XRD, mechanical, TEM and SEM were given below.

XRD raw diffraction image in transmission for extruded K10-HP filament of 1.7 mm and microfilament of about 0.35mm were shown Fig.9.

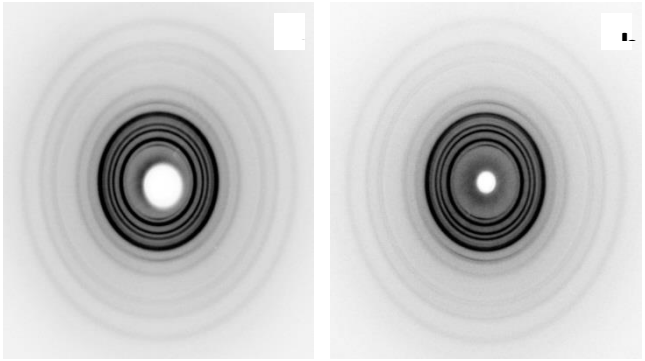

Fig.9 X-ray transmission image of HP500 with 10% kaolinite (a) filament of 1.7 mm diameter (b) microfilament of 0.35 mm diameter.

As observed from these XRD images of filaments for 3D printing and microfilaments does not show clear difference in crystallography. From this we can understand that there is no drawing effect during extrusion through a nozzle, the filaments in 3D printing only undergoes re-melting and re-shaping. Thus there is no orientation in terms of structure of polymer. If the polypropylene shows a strong orientation along the chains axis, the kaolinite texture is characterized by a fiber like orientation with the basal/faulted planes perpendicular to it (001 faulted plane). However here there is no visible orientation difference as that of observed in drawn fibers.

3.8 Mechanical properties of microfilaments and bulk filaments

Mechanical properties of microfilaments and filaments for 3D printing were analyzed and compared to each other. Representative stress – strain curves of the quasi-static tensile tests of neat HP, K10-HP and K20-HP filaments for 3D printing tested by using a load of 1 kN are shown in Fig.10 (a). Also main mechanical properties of neat HP, K10-HP and K20-HP filaments for 3D printing are described in Table 9.

Similarly mechanical properties of micro filaments which extruded through a hot nozzle of 350 micron (microfilaments) on PP adhesive strips coated bed were analyzed. Representative stress-strain curves of neat HP, K10-HP and K20-HPmicrofilamentstested at a load of 100 N are shown in Fig.10 (b). Mechanical properties of neat HP, K10-HP and K20-HP nanocomposites of microfilaments were also summarized in Table 9.

As observed from stress-strain curves of filaments for 3D printing, addition of 10wt% kaolinite enhance the mechanical properties other than strain at break compared to neat HP polypropylene. But at higher composition of 20wt% of kaolinite, less mechanical properties may be due to larger agglomerates formation which could be evaluated in microstructural study and increase in other defects.

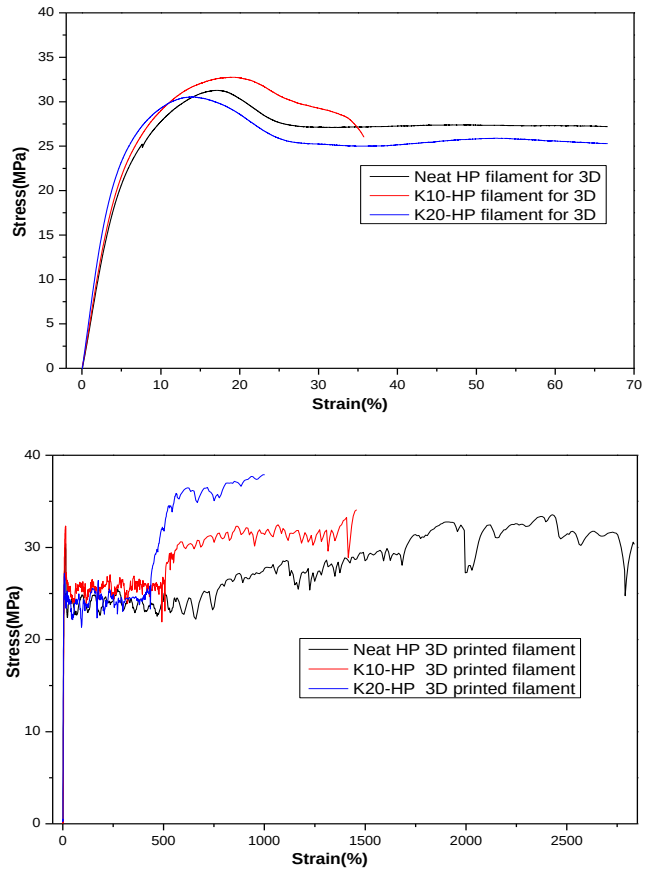

Fig.10 Representative of stress strain of neat HP, K10-HP and K20-HP (a) filaments for 3D printing (b) microfilaments.

Table 9 Mechanical properties of neat HP, K10-HP and 20K-HP filaments for 3D printing and microfilaments.

Filament Type	*Material*	*Elastic Modulus (GPa)*	*Stress at yield (MPa)*	*Strain at yield stress (%)*	*Stress at break (MPa)*	*Strain at break (%)*
Filaments for 3D printing	Neat HP	0.50 ± 0.2	27.0 ± 3.8	14.9 ± 2.3	24.7 ± 2.8	66.7 ± 0.1
	K10-HP	0.44 ± 0.0	30.9± 1.7	18.0 ± 3.0	23.5 ± 1.4	29.6 ± 7.5
	K20-HP	0.47 ± 0.1	27.4 ± 2.8	14.1 ± 2.5	21.2 ± 4.0	56.8 ± 17.0
Microfilaments	Neat HP	0.74 ± 0.1	31.3 ± 4.4	12.9 ± 0.8	37.4 ± 10.2	2178 ± 590
	K10-HP	0.92 ± 0.0	32.1± 0.5	12.7 ± 2.6	32.7 ± 1.1	1598 ± 642
	K20-HP	0.91 ± 0.1	27.2 ± 0.1	6.7 ± 1.5	30.5 ± 10.1	1332 ± 395

Thus considering mechanical properties and comparing the two filaments; the modulus of filaments from 3D printing of K10-HP (0.92 GPa) and K20-HP(0.91GPa) shows higher value compared to neat HP (0.74 GPa) polypropylene. But tensile modulus of kaolinite filled filaments for 3D printing shows the tendency of decreasing with the kaolinite content, which is 0.5 GPa for neat HP to about 0.44 GPa for K10-HP and 0.47 GPa for K20-HP nanocomposites. This decrease may results from the bulk size of filaments, because as the size increases agglomerates and other defects in the filament chain increases.

Considering properties at yield, the strength of K10-HP of about 32 MPa, 31 MPa for neat HP and lower strength of about 27 MPa for K20-HPwas found for filaments from 3D printing. But the stress at yield of filaments for 3D printingwas increased to about 31 MPa with K10-HP and almost the same of about 27 MPa for neat HP and K20-HP. Strain at yield shows a decrease with kaolinite content for microfilaments while it was increasing with K10-HP and almost same strain for neat HP and K20-HP filaments for 3D printing.

Looking mechanical properties at break, stress at break and strain at break for microfilaments shows decrease with kaolinite content. Similarlyfilaments for 3D printing shows a decrease in strength at break with kaolinite content while the strain at break was highly decreasing with kaolinite content of 10wt% relative to neat HP polypropylene. Filaments for 3D printing shows relatively lower strength and strain at break compared to microfilaments. Thus in 3D extrusion through a nozzle there is re-orientation of kaolinite particles and decreases the probability of defects formation and improves mechanical properties. This concept was observed under morphology study by FESEM and TEM.

3.9 Morphology

The dispersion of kaolinite in filaments for 3D printing and microfilaments of K10-HP and K20-HP was evaluated by FESEM on the fractured surfaces of the filaments in nitrogen and TEM on ultramicrotomed cross sections as summarised in Table 10. Comparison of fillers dispersion in the K10-HP and K20-HP filaments for 3D printing with microfilaments by using FESEM micrographs were shown in Fig.11(a)-(d), respectively.

Table 10 Comparison of morphology of filament and microfilaments at different kaolinite content by means of FESEM and TEM.

EM	Sample	K10	K20
FESEM	Filament	X15, 000	X15,000
	Microfilament	X15, 000	X15, 000
TEM	Filament	X 1 micron	X 1 micron
	Microfilament	X 1 micron	X 1 micron

TEM morphology of filaments for 3D printing and microfilaments of K10-HP and K20-HP are shown in Fig.12. As shown in these figures almost the amount of kaolinite content is almost the same, but due to re-melting and re-shaping during extrusion through nozzle more uniform distribution of kaolinite were observed in microfilaments, Fig.12(b).

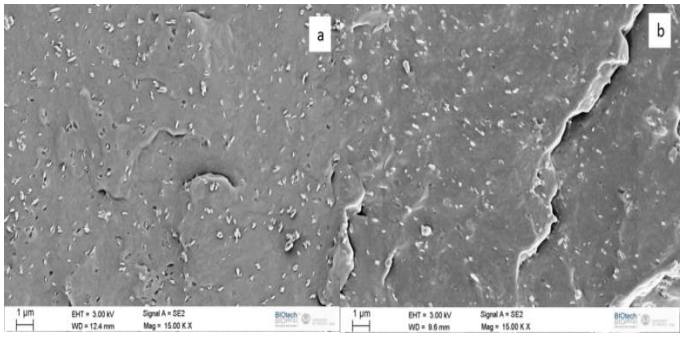

Fig.11 (a-b) FESEM micrographs of the fractured surface of K10-HP kaolin-filled PP (X15,000) (a) filament for 3D printing and (b) microfilament.

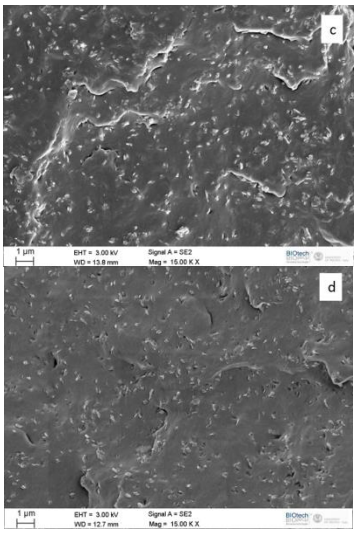

Fig.11(c-d) FESEM micrographs of the fractured surface of K20-HP kaolin-filled PP (X15,000) (c) filament for 3D printing and (d) microfilament.

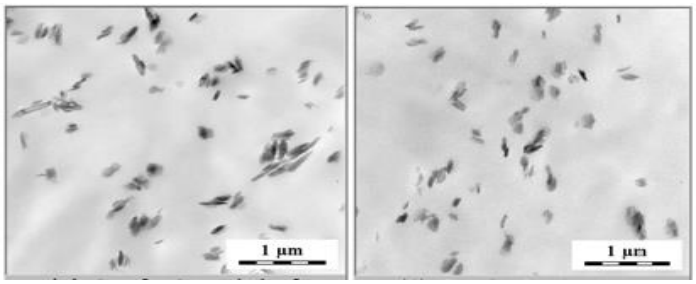

Fig.12 (a-b). TEM micrographs of K10-HP (a) filaments for 3D printing and (b) microfilament RO = 25 (Re-orientation)

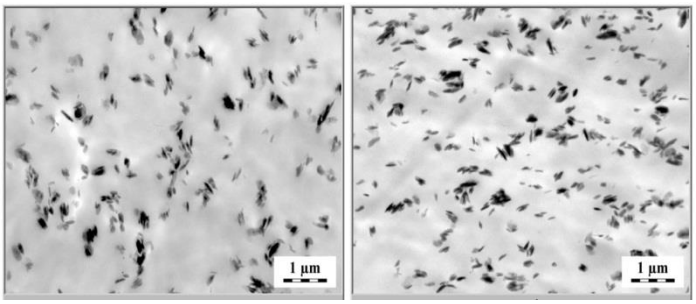

Figure 3.28(c-d). TEM micrographs of K20-HP (a) filaments for 3D printing (b) microfilament RO = 25 (Re-orientation)

TEM micrographs also evidence that kaolinite nanoparticles are quite well fixed in the PP matrix even if they are agglomerated, because the matrix penetrates inside the agglomerates and the interface is not sharp but diffuse, which indicates good interfacial adhesion.

Both FESEM and TEM showgood dispersion other than tendency of formation of small agglomerate due to hydrogen bonds formed between kaolinite particles. From morphological view of FESEM micrographs filaments for 3D printing and microfilaments seems to have the same filler amount and the lack of dispersion properties could be due to absence of any drawing effect, but from TEM micrographs it is possible to observe disaggregation of aggregates in microfilaments which was well observed in K10-HP filament. TEM micrographs of filaments of K20-HP shows overcrowded kaolinite particles; however it is possible to observe improvement of dispersion in microfilaments (Fig.12d) compared to filaments for 3D printing. The effects of re-melting and re-shaping through 3D printer nozzle were seen very well in mechanical properties.

3.10 Dumbbell Shape 3D Printed Samples. Production and Characterization.

Dumbbell shape sample were printed after the designing the specimen by CAD and slices into pieces by slic3r software. The main parameters set to build structures are: infill types of concentric, object infill of 100%, layer height of 0.20 mm, infill angle/raster of $45^0$and 10 total numbers of layers with nozzle diameter of 0.35 mm. Schematic steps of building dumbbell structures were shown in Fig.13.

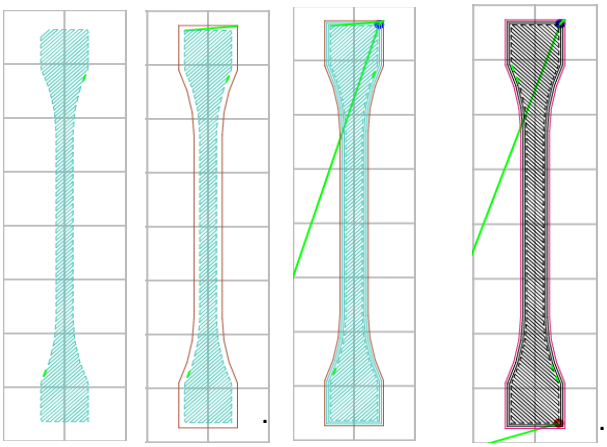

Fig.13 Schematic diagram of dumbbell structures build-up by 3D printing process: (a)-(c) steps to build first layer (d) second layer (perpendicular to first layer).

An enlarged sample of K10-HP 3D printed dumbbell with the given parameters was shown in Fig.14. As shown on fig.14 dumbbell shape structures of neat HP, K10-HP and K20-HP is built in step-wise layer by layer. Dumbbell sample of 2mm thickness was built from 10 layers of each 0.2 mm thickness where every successive layer is perpendicular to each other at 45^0. There were clearly observed cavity formed during the laying of layers as it can be seen in Figure

3.30, which in turn results in decrease of properties of sample.

Fig.14 3D printed dumbbell sample of K10-HP (x3).

As cooling proceed from T_m to room temp, it will results in high warping stresses compared to typical 3D printing materials. It was found that HP and K-HP nanocomposites have also very poor adhesion behaviour on a heated 3D printing bed and results in *banana-shape* specimens. This effect results from low surface-energy properties of PP and its composites, low adherence properties to bed because PP doesn't want to stick too much of anything except itself. Fig.15 shows a representative *banana-shape* sample of 3D printed dumbbell on a bare heated bed.

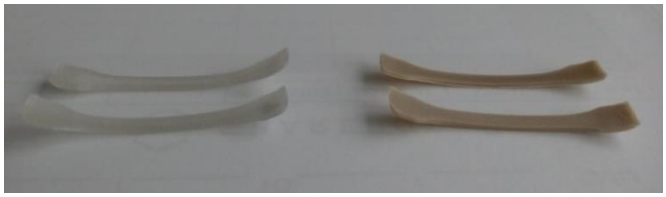

Fig.15 3D printed sample of dumbbell shape of neat HP and K10-HP on a heated bed.

To improve this problem a new technique was introduced by finding a material made from polypropylene on which the sample would be printed. Accordingly a 3D printing bed was coated with packaging adhesive strips (which are made up of PP) before starting printing process, with adhesive side facing down to the bed.

As a flow or creep rate of HP and its nanocomposites is not meaningful over the duration of fused deposition print, appropriate temperature and deposition speed for neat HP and K-HP nanocomposites was controlled to reduce the problems. Thus temperature of nozzle and bed for neat HP is set to be higher 240 ^{0}C and 90 ^{0}C, respectively while it is set to 230 for nozzle and 80 for bed in case of K10-HP and K20-HP. The decrease in processing temperature is needed due to the increase in melt flow index observed with increase of kaolinite content. Also to avoid fast cooling and higher shrinkage a technique of covering 3D printing surround by thick clothes and hard papers was tried. This technique is assumed to adhere one layer to next layer and to produce compact sample with reduced cavity between layers. Fig.16 shows the 3D printed dumbbell shape samples printed on adhesive strips coated heated bed.

Looking at Fig.16, it is easy to understand improvement in shrinkage of 3D printed sample of HP and K10-HP compared to the one printed on bare bed (Fig.15). Also comparing the design size and printed samples, the samples printed on a coated bed gives higher accuracy in all direction size of about 95% compared to 90% for samples printed on bare bed.

Fig.16 3D printed sample of dumbbell shape of neat PP and PP-K10 on adhesive strips coated heated bed.

Equivalent diameters for dumbbell shape materials were calculated from itsbase width and thickness by the formula; $A = \pi r^2$ where r can be calculated from the cross-sectional area of 3D printed sample and equivalent diameter is twice of the calculated radius. The calculated diameter is only for bulk 3D printed samples without considering the cavity and holes observed in the structures.

3.11 Printed dumbbells sample characterization

DSC analysis of neat HP, K10-HPand K20-HP was performed on 3D printed samples to provide quantitative evaluation of the crystallization behaviour. The DSC thermograms curves of neat HP, K10-HPand K20-HP 3D printed samples are shown in Fig.17. Similar to filaments for 3D printing crystallization temperatures increase with the increase of kaolinite content and melting temperature is almost the same for neat HP, K10-HP and K20-HP filled 3D printed filaments. The crystallinity content of filaments after cooling is higher than the first melting $\mathcal{X}_c$ displayed. Crystallinity after cooling is almost same for neat HP and K-HP filled 3D printed samples. This earlier crystallization phenomenon can be interpreted as the result of an increase in nucleation activities.

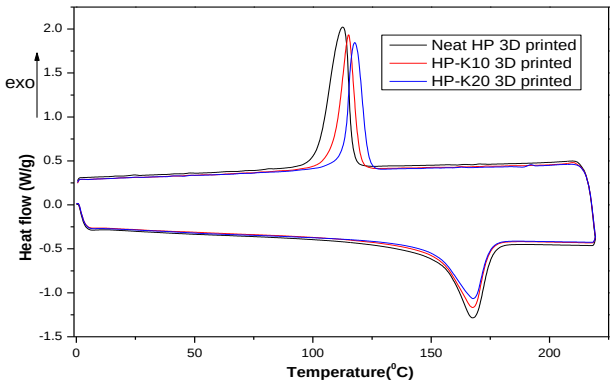

Fig.17 DSC thermograms of neat HP, K10-HP and K20-HP 3D printed samples.

From these curves parameters for crystallization analysis such as the melting temperature (T_m), the crystallization temperatures (T_c) can be obtained. The degree of crystallinity ($\mathcal{X}c$) of HP and K-HP nanocomposites 3D printed samples was calculated.

Melting process induces the molecular chains mobility of PP, and reduces the free energy barrier for crystallites formation which is able to accelerate the rate of crystallization. The crystallinity content after cooling is almost the same for both neat HP and K-HP filled filaments. These results investigate that after filament productions the crystallinity content does not change and the incorporation of kaolinite acts as heterogeneous nucleation center to the PP matrix.

Table 11. Results of the DSC analysis: melting temperature (Tm), crystallinity content (Xc) and crystallization temperature (Tc) for neat HP, K10-HP and K20-HP 3D printed samples.

Sample Composition	*1st melting temp.*		*Crystallization temp.*		*2nd melting temp.*		*Crystallinity Content (%)*	
	peak (°C)	*integral (J/g)*	*peak (°C)*	*integral (J/g)*	*peak (°C)*	*integral (J/g)*	*1st Melting*	*After Cooling*
Neat HP	167	94	112	97	165	97	46	47
10K-HP	168	81	116	87	165	87	42	46
20K-HP	168	72	120	79	165	79	42	46

Mechanical properties of 3D-printed dumbbell samples can be influenced by many factors, such as layer thickness, fill angle, build orientation, fill pattern, air gap and model build temperature.3D printed sample of dumbbell build according to the given parameters above were tested and representative stress-strain curves of neat HP, K10-HP and K20-HPsamples are shown in Fig.18. Mechanical properties of neat HP, K10-HP and K20-HP nanocomposites of dumbbell shape samples were summarized in Table 12.

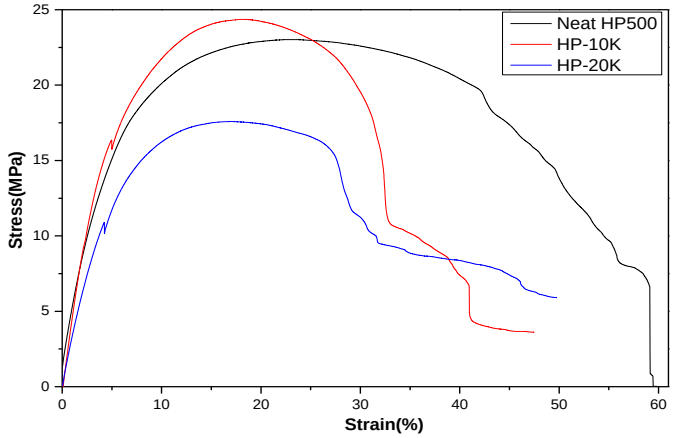

Fig.18 Representative of stress strain of 3D printed dumbbell shape of neat HP, K10-HP and K20-HP samples.

Tensile test results summarized in Table 12 shows that K10-HP composition dumbbell has higher modulus and yield stress, but lower strain at break relative to neat HP. However the composition of K20-HP has relatively lower modulus, yield stress and strain at break which could be due to agglomerates formation, higher cavity and lower adhesion of different layers during the layer deposition. Also as it is shown in Fig.18, breaking of the dumbbell is step-wise which looks like the breakdown of composite material. From literature search there is no standard for the evaluation of build orientation-based mechanical performance currently; such analysis has typically been achieved through the fabrication and investigation of tensile and other tests which were printed in different build orientations. There are also multiple tensile test specimen geometries specified in the ASTM D638 standard for the tensile testing of polymer/composite materials and understanding which specimen geometry works best for 3D printing is not currently well understood.

Table 12 Mechanical properties of neat HP and HP-kaolinite nanocomposites of 3D printed dumbbell samples.

Samples	*Elastic Modulus (GPa)*	*Yield stress (MPa)*	*Strain at yield stress (%)*	*Stress at break (MPa)*	*Strain at break (%)*
Neat HP	0.39 ± 0.03	20.6 ± 2.1	21.7 ± 1.1	14.2 ± 1.0	56.0 ± 4.5
K10-HP	0.51 ± 0.00	24.0 ± 0.4	18.4 ± 0.2	25.18 ± 1.0	33.2 ± 3.8
K20-HP	0.35 ± 0.02	18.2 ± 0.8	15.8 ± 1.2	15.58 ± 0.2	41.3 ± 9.5

Morphology study of 3D printed dumbbell of neat HP, K10-HP and K20-HP shows that there is a cavity formation between layers at the edge and infill which is perpendicular to one another at 45^0. Fig19 shows SEM micrograph of K10-HP and K20-HP dumbbell shape samples.

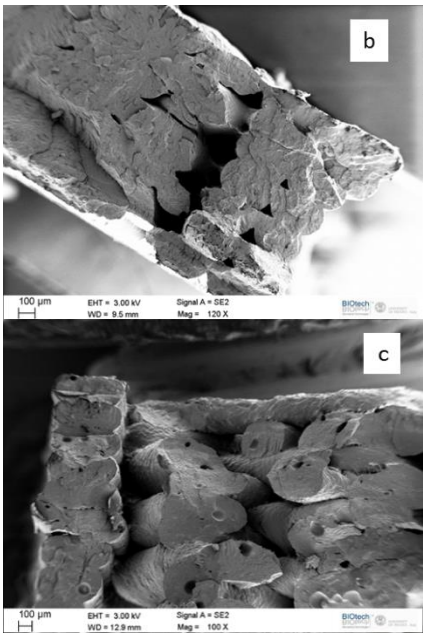

Fig.19 FESEM micrograph of 3D printed dumbbell fractured surface of kaolin-filled PP (a) K10-HP of failure between layers (X120) (b) K20-HP (X100).

As observed in FESEM micrograph,figure 3.36,it is possible to see the numbers of layers used to build dumbbell shape samples. In Figure 3.35(a), there is a large hole which seems a failure (delamination), separation of layers from each other's between layers of 3D printed material. This failure could be due to lower adhesion of PP to kaolinite or insufficiency in filling during printing process. According to the view from 3D printed dumbbell there was higher cavity formation between layers especially in K20-HP dumbbell sample. Formation of many cavities in could results decrease in mechanical properties and this approves the reason for observed decrease of mechanical properties of K20-HP.Comparing the dumbbell sample observed the adhesion between PP-PP is better compared to its nanocomposites as shown in Fig.20.

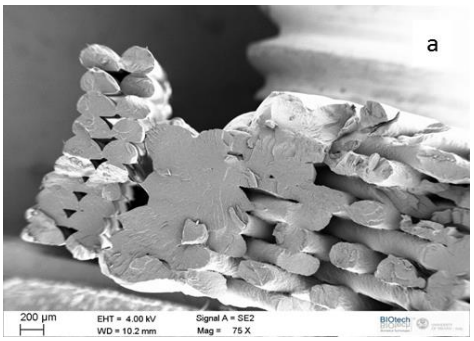

Fig.20 FESEM micrograph of 3D printed dumbbell fractured surface of neat HP (X75).

4. SUMMARY AND CONCLUSION

Filaments for Additive Manufacturing of neat HP, K10-HP and K20-HP of about 1.7 mm were extruded and its properties are analysed by different techniques. Melt flow index of filaments for 3D printing reveals that MFI values increased with the percentage of kaolinite in the polymer matrix, with a linear dependence on the PP-kaolinite composition. Thus the maximum MFI value of 2.46 g/10min was obtained for K20-HP compared to 1.96 g/10min for neat HP polypropylene.

Bulk properties of filaments were compared in term of density, and it evidenced a direct dependence of density on the composition. The higher the kaolinite content, the higher the density measured in between the density 0.8918 g/cm^3 of neat HP polypropylene and 0.9854 g/cm^3 for the density of K20-HP. The measured density is lower than theoretical density due to observed cavity and other defects. TGA of filaments for 3D printing performed in nitrogen gas and air atmospheres shows three different zones in which there is no significant weight loss, high mass loss due to thermal decomposition of polymer matrix and no significant mass loss since the residuals are not decomposed. The decomposition of the matrix in N_2 gas is slower because it prevents undesirable chemical reactions from taking place. Thermal decomposition temperature at 5%, 10% and maximum weight loss of the neat HP and its nanocomposites shows an increase with increasing kaolinite content. This effect results due to kaolinite act as physical barriers to hinder the transport of volatile decomposed products. The residual mass at 700°C was almost equal in both testing medium. This proves that incorporation of kaolinite into the

polymer matrix enhances the thermal stability of polypropylene composite.

DSC results of neat HP, K10-HP and K20-HP nanocomposites of filaments for additive manufacturing and microfilaments shows increase in crystallization temperatures, almost the same melting temperature and crystallinity content with increase of kaolinite content. The increase in crystallinity content after cooling is also observed compared to the first melting crystallinity content , χ_c.This crystallization phenomenon can be interpreted as the result of an increase in nucleation activities. Melting process induces the molecular chains mobility of PP, and reduces the free energy barrier for crystallites formation which is able to accelerate the rate of crystallization.DSC analysis of neat HP, K10-HP and K20-HP filaments for 3D printing and microfilaments are summarised for single heating-cooling cycle in Table 13.

Filament type	*Composi-tion*	*Melting temp.*		*Crystallization temp.*		*Crystallinity Content (%)*
		peak (°C)	*integral (J/g)*	*peak (°C)*	*integral (J/g)*	
Filaments for 3D printing	Neat HP	167	83.2	113	96.7	40.2
	K10-HP	167	81.0	116	86.6	42.4
	K20-HP	166	73.9	119	78.0	42.7
Microfilaments	Neat HP	167	94.3	112	97.1	45.5
	K10-HP	168	81.3	116	87.0	42.4
	K20-HP	168	71.9	120	79.2	41.6

Table 13 Summary of DSC analysis of filaments for 3D printing and microfilaments.

Melting temperatures (Tm) is almost the samefor neat HP and kaolinite filled HP in both filaments for 3D printing and microfilaments with the increase of kaolinite content, even though microfilaments of K20-HP shows slight higher value. From the cooling stage, it was noticeable that crystallization temperatures of kaolinite filled filament were also higher for K20-HP, i.e. about 119.6°C for versus 112.4°C for neat HP of microfilaments. This clearly implies that the incorporation of kaolinite results in the heterogeneous nucleation to the HP PP matrix.

Crystallinity content in filaments for 3D printing slightly increases with kaolinite content and it decreases in microfilaments with increase in kaolinite content and no clear influence of kaolinite presence was observed. Literature data reported various effects of nanofiller on crystallization temperature and crystallinity content of polyolefin matrix, showing negligible [13], or significant [14] effect, in dependence on both processing and composition. In this case, the crystallinity of nanofilled polypropylene was slightly higher than neat HPin both 10 and 20wt% of kaolinite in filaments for 3D printing and lower in microfilaments, whereas the crystallization temperature increased with kaolinite content. Comparing these results with the literature references, it is difficult to have clear image of the effect of kaolinite on the crystallinity behaviour of polypropylene matrix. It can be said that kaolinite nanoparticles plays a marginal role on the crystallization behaviour of the PP matrix and the limited influence on the matrix properties were probably associated to their dispersion state [15].

Mechanical properties of filaments for 3D printing, microfilaments and 3D printed dumbbell shape sample were summarized in Fig.21 and Table 14.

Table 14 Summary of mechanical properties of filaments for 3D printing, microfilaments and 3D printed dumbbell.

Filament Type	*Material*	*Tensile Modulus (GPa)*	*Stress atbreak, σ_b(MPa)*	*Strain at break, ε_b(%)*
Filaments for 3D printing	Neat HP	0.50 ± 0.16	24.67 ± 2.8	66.7 ± 0.1
	K10-HP	0.44 ± 0.00	23.49 ± 1.4	29.6 ± 7.5
	K20-HP	0.47 ± 0.10	21.22 ± 4.0	56.8 ± 17.0
Microfilaments	Neat HP	0.74 ± 0.10	37.42 ± 10.2	2178.3 ± 590.5
	K10-HP	0.92 ± 0.00	32.66 ± 1.1	1598.1 ± 641.8
	K20-HP	0.91 ± 0.10	30.51 ± 10.1	1332.3 ± 394.9
3D printed dumbbell	Neat HP	0.39 ± 0.03	14.24 ± 0.98	56.00 ± 4.5
	K10-HP	0.51 ± 0.00	25.18 ± 0.98	33.2 ± 3.8
	K20-HP	0.35 ± 0.02	15.58 ± 0.17	41.3 ± 9.5

Comparing mechanical properties of tensile modulus, stress at break and strain at break of filaments for 3D printing and 3D printed dumbbell sample shows lower value than that of microfilaments. The observed decrease in mechanical properties was due to filaments and dumbbell bulk size which results in increase of agglomerates, cavity and other defects in the structure. The formation of larger cavity and holes in dumbbell shape sample were clearly seen on specimen and under morphological study. Similarly formations of holes were also observed on filaments for 3D printing under FESEM. But in case of microfilaments the probability of formation of defects decrease due to re-melting and re-orientation taking place in nozzle and decrease in size of filaments.

Elastic modulus of filaments for 3D printing were decreasing with kaolinite content compared to neat HP, while it increases with kaolinite addition for filaments from 3D

printing and for dumbbell samples it increases for K10-HP and decreases for K20-HP compared to neat HP polypropylene. Here it is necessary to remember that the mechanical properties of 3D printed sample do not depend only on kaolinite content but also many factors such as fill angle, direction of building and adhesion between layers during production of samples. Stress at break decreases with kaolinite content in both filaments for 3D printing and microfilaments but in dumbbell sample it was observed higher value for K10-HP than that of neat HP. Strain at break for microfilaments decreases with kaolinite content but in other cases it does not depend too much on kaolinite content, specially strain at break for K10-HP is lower than K20-HP in filaments for 3D printing and dumbbell samples. The stress-strain curves of 3D printed dumbbells shows a sequential break down. From comparative results given above it is possible to conclude that 3D printed dumbbell samples have lower mechanical properties due to higher cavity formed between layers during the production.

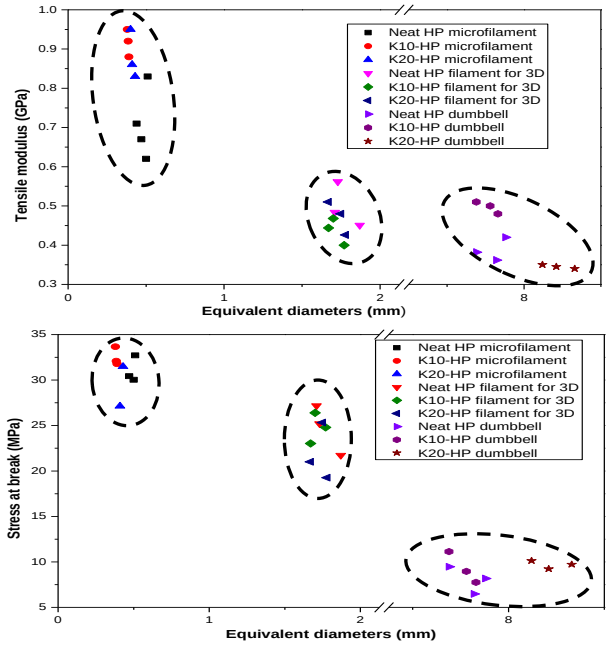

Fig.21 Mechanical properties of filaments for 3D printing, microfilaments and 3D printed dumbbell (a) tensile modulus versus equivalent diameter (b) stress at break versus equivalent diameter.

XRD results of filaments for 3D printing and microfilaments sample don't show much difference in texture and crystal arrangement. But from TEM micrographs it is possible to observe disaggregation of aggregates in microfilaments which was well observed in K10-HP filament. Microstructural study by FESEM reveals good dispersion of kaolinite even though there is formation of agglomerates. FESEM micrographs also show existence of holes and subsequent plastic deformation in the morphology due to weak interfacial adhesion between PP and kaolinite. Amount of holes also implies the content of kaolinite, i.e. the numbers of holes formed in K20-HP is much higher than that of K10-HP. The improvement of dispersion of kaolinite in polypropylene was not clearly seen in filaments for 3D printing and microfilaments may be due to absence of any drawing effect during extrusion though a 3D printer nozzle, only re-melting and re-shaping taking place. FESEM micrographs of 3D printed dumbbells shows a formation of larger cavity between layers which results in decrease of mechanical properties.

3D printing of neat PP and kaolinite-PP nanocomposites is difficult with parameters used for normal printable materials. Semi-crystallinity properties of PP and its nanocomposites results in build-up of thermal contraction stresses as it is cooled below melting temperature and poor adhesion behavior on heated bed. Coating of 3D printer bed with PP materials improves poor adhesion behavior between PP and heated bed. Also to obtain a good quality of 3D printed sample setting temperature of nozzle and bed in decreasing manner with increase of kaolinite content was required because of observed increase in MFI with kaolinite contents of filaments.TEM analysis shows disaggregation of aggregates due to re-melting, re-shaping and some reorientation during extruding through the nozzle in microfilaments. Morphological study of samples show formation of larger cavity and holes in 3D printed dumbbell shape sample which results in decrease of mechanical properties. Mechanical properties of 3D printed sample of K10-HP shows improvement compared to neat HP.

Mechanical properties of fibers, filaments for 3D printing, microfilaments and 3D printed dumbbell versus equivalent diameter were summarized in Fig.15 and Fig.16. This positive effect of fibers observed in terms of modulus and stress at break was attributed to the good dispersion and alignment of nanoparticles induced during drawing process, which promotes molecular orientation and crystallization of the amorphous region. Decrease in mechanical properties observed for high kaolinite content was due to formation of larger agglomerates. The observed decrease in modulus and stress at break of filaments for 3D printing and 3D printed dumbbell was due to their bulk size which tendency of agglomerates, cavity and other defects formation increase in the structure.

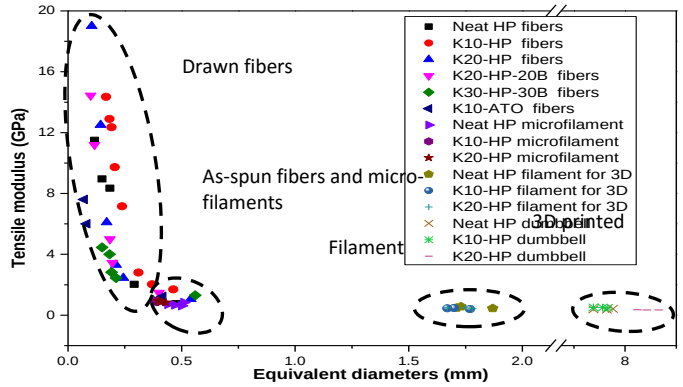

Fig. 15 Tensile modulus of filaments for 3D printing, microfilaments and 3D printed dumbbell as a function of equivalent diameter

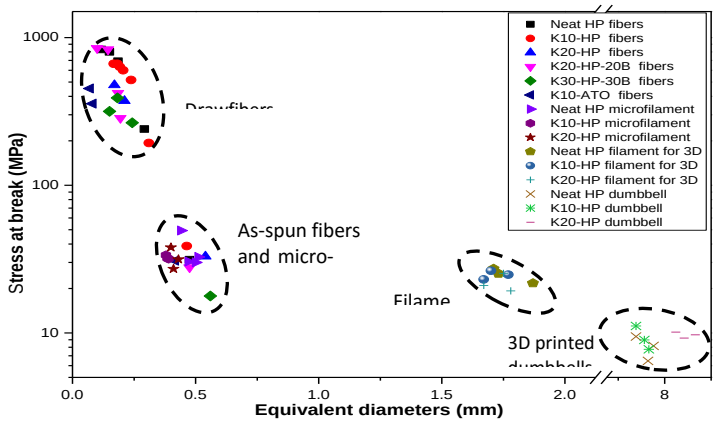

Fig. 16 Stress at break of filaments for 3D printing, microfilaments and 3D printed dumbbell as a function of equivalent diameter.

Incorporation of kaolinite into a polypropylene matrix enhanced its rheological properties, thermal stability and mechanical properties in both spun fibers and 3D printed samples. Therefore kaolinite-PP nanocomposites can be used for materials and processing requires higher-performance in stiffness and temperature compared to neat PP such as food packaging, automotive parts and other applications.

REFERENCES

[1] Wong KV, Hernandez A. A review of additive manufacturing. ISRN MechEng, 1–10, 2012.

[2] Durgun I, Ertan R. Experimental investigation of FDM process for improvement of mechanical properties and production cost. Rapid Prototyp J, 20(3), 228–35, 2014.

[3] Krawczak P. Additive manufacturing of plastic and polymer composite parts, promises and challenges of 3D-printing. Exp Pol Lett, 9(11), 959, 2015.

[4] https://info.aiaa.org/SC/ETC/MSSubCommittee/AliceChow_3DPrintingChangetheWorld_April2012.pdf.

[5] Zhai Y., Lados D.A., LaGoy J.L., Additive manufacturing: making imagination the major limitation, JOM 66, 808–816, 2014.

[6] Cooper D.E., Stanford M., Kibble K.A., Gibbons G.J., Additive manufacturing for product improvement at Red Bull technology, Mater. Des. 41, 226–230, 2012.

[7] Drummer D., Cifuentes-Cuéllar S., Rietzel D., Suitability of PLA/TCP for fused deposition modeling, Rapid Prototyp. J. 18, 500–507, 2012.

[8] Domingos M., Chiellini F., Gloria A., Ambrosio L., Bartolo P., Chiellini E., Effect of process parameters on the morphological and mechanical properties of 3D Bioextruded poly(e-caprolactone) scaffolds, Rapid Prototyp. J. 18, 56–67, 2012.

[9] Carneiro O.S., Silva A.F., Gomes R., Fused deposition modeling with polypropylene, Mater . Des, 83, 768–776, 2015.

[10] Sithiprumnea D., Fambri L., Pegoretti A., Fused deposition modelling with ABS–graphene nanocomposites. Composites: Part A, 85, 181–191, 2016.

[11] https://www.sharebot.it/

[12] ASTM D 1238 - 04c, Standard test method for melt flow rates of thermoplastics by extrusion plastometer.

[13] Deshmane C.Yuan Q.Perkins R.S.Misra R.D.K., On striking variation in impact toughness of polyethylene-clay and polypropylene-clay nanocomposite systems: The effect of clay-polymer interaction. Material Science & Engineering, A, 458, 150-157, 2007.

[14] Xu J.-T., Wang Q., Fan Z.-Q., Non-isothermal crystallization kinetics of exfoliated and intercalated polyethylene/montmorillonite nanocomposites prepared by in situ polymerization. European Polymer Journal, 41, 12, 3011-3017, 2005.

[15] D'Amato,M.,Dorigato A., Fambri L., Pegoretti A., High performance polyethylene nanocomposite fibers. eXPRESS Polymer Letters, 6,12, 954-964, 2012.